



저작자표시-비영리-변경금지 2.0 대한민국

이용자는 아래의 조건을 따르는 경우에 한하여 자유롭게

- 이 저작물을 복제, 배포, 전송, 전시, 공연 및 방송할 수 있습니다.

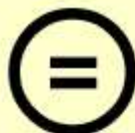
다음과 같은 조건을 따라야 합니다:



**저작자표시.** 귀하는 원저작자를 표시하여야 합니다.



**비영리.** 귀하는 이 저작물을 영리 목적으로 이용할 수 없습니다.



**변경금지.** 귀하는 이 저작물을 개작, 변형 또는 가공할 수 없습니다.

- 귀하는, 이 저작물의 재이용이나 배포의 경우, 이 저작물에 적용된 이용허락조건을 명확하게 나타내어야 합니다.
- 저작권자로부터 별도의 허가를 받으면 이러한 조건들은 적용되지 않습니다.

저작권법에 따른 이용자의 권리는 위의 내용에 의하여 영향을 받지 않습니다.

이것은 [이용허락규약\(Legal Code\)](#)을 이해하기 쉽게 요약한 것입니다.

[Disclaimer](#)

Thesis for the Degree of Master of Science

**Thickness and Strain Dependence of  
Magnetic Properties of Ultrathin  
Fe/Ni Films on Cu(001) Substrate**



by

Dongyoo Kim

Department of Physics

The Graduate School

Pukyong National University

February 2008

Thickness and Strain dependence of Magnetic Properties  
of Ultrathin Fe/Ni Films on Cu(001) Substrate

Fe/Ni 초박막에서의  
두께 변화와 변형에 따른 자기적 특성 연구

Advisor : Jisang Hong

by

Dongyoo Kim

A thesis submitted in partial fulfillment of the requirements  
for the degree of Master of Science

in the Department of Physics, Graduate School,  
Pukyong National University

February 2008

Thickness and Strain dependence of Magnetic Properties  
of Ultrathin Fe/Ni Films on Cu(001) Substrate

A dissertation

by

Dongyoo Kim

Approved as to style and content by :

---

Dr. Chanyong Hwang  
Chair of Committee

---

Prof. Byung Kee Moon  
Member of Committee

---

Prof. Jisang Hong  
Member of Committee

## Contents

Abstract .....	iii
Chapter 1. Introduction .....	1
Chapter 2. Basic Theory .....	4
2.1 Magnetic anisotropy energy .....	4
2.1.1 Introduction .....	4
2.1.2 Phenomenology of Magnetic Anisotropy .....	5
2.1.3 Anisotropy Arising from Dipolar Interactions .....	7
2.1.4 Anisotropy Arising from Spin-Orbit Coupling .....	9
2.2 X-ray magnetic circular dichroism (XMCD) .....	12
Chapter 3. FLAPW method .....	14
3.1 The Density Functional Theory .....	14
3.1.1 The Density Functional Theory .....	14
3.1.2 Spin-polarized density functional theory .....	17
3.1.3 Approximation method for exchange-correlation energy .....	17
3.2 The FLAPW Method .....	19
3.2.1 Introduction .....	19
3.2.2 The FLAPW method and Basis-set .....	20

Chapter 4. Computatinal Results .....	23
4.1 Numerical Method .....	23
4.2 Numerical Results and Discussion .....	24
4.2.1 Structural Feature .....	24
4.2.2 Magnetic Moment .....	28
4.2.3 Density of State .....	30
4.2.4 Magnetic Anisotropy Energy .....	34
4.2.5 XMCD and Sum Rule .....	40
4.3 Conclusion .....	46
Reference .....	47



Thickness and Strain Dependent Magnetic Properties of Ultrathin Fe/Ni Film  
on Cu(001) Substrate

Dongyoo Kim

Department of Physics, Graduate School  
Pukyong National University

Abstract

Using the full potential linearized augmented plane wave (FLAPW) method, the magnetic properties of ultrathin Fe/Ni films grown on Cu(001) surface have been investigated. We have varied both Ni and Fe film thickness and also have explored the strain effect on the magnetic anisotropy. For surface Fe atom, a typical surface enhancement of spin magnetic moment has been observed while the magnetic moments of other constituents are rather insensitive to the strain effect. Nonetheless, we have realized that the direction of magnetization is significantly affected by the strain factor. For instance, the Fe/Ni films always have perpendicular magnetization provided that they grown on Cu (001) lattice constant. However, we have obtained a spin reorientation transition (SRT) phenomenon in the presence of strain effect. In addition, the theoretically calculated X-ray absorption spectroscopy (XAS) and X-ray magnetic circular dichroism (XMCD) are presented. Moreover, the validity of XMCD sum rule has been explored.

# Chapter 1 Introduction.

The magnetic properties of thin films and magnetic multi-layers have long been extensively investigated since last decades. In these days, the atomic manipulation technique has been remarkably improved and this makes it possible to grow new structures in an artificial way and tailor the magnetic properties of materials. It is well known that the magnetic property is very sensitive to the change of electronic structure. In ultrathin films, the influence of alteration of electronic structure on the magnetic property of sample will definitely play an important role. Indeed, the effect will be most clearly seen in nano scale structure. As a result, to date, a great amount of research effort has been focusing on the studies of ultrathin magnetic films due to their physical properties and promise for potential spintronics device application [1-3].

Among the many magnetic properties in ultrathin films, the central issue is the magnetic anisotropy that determines the direction of magnetization. In particular, the spin reorientation transition (SRT) has attracted great attention in the field of theoretical and experimental studies. The Ni/Cu(001) is well known as a prototype of SRT structure. It has been known that the Ni/Cu(001) displays SRT twice depending on the Ni thickness. For instance, the change of magnetization from in-plane to perpendicular to the surface is observed approximately at the Ni thickness of 10 monolayers (ML) and another SRT is found at roughly 40ML Ni thickness. The similar phenomena are also found in other structures such as Fe/Co/Cu and Fe-Co alloys. Also, the SRT is substantially influenced by interface and surface contributions, thus many attempts have been performed to manipulate the magnetic properties of magnetic thin films adding capping layer or surfactant elements [4-9]. Very recently, the thickness dependent magnetic anisotropy in Fe/Ni/Cu(001) films have been

explored by two different groups [10, 11]. They, however, have shown different results. Several factors can affect the magnetic anisotropy of materials such as strain, interfaced and surface effects. It is of interest of investigate the physical origin of these thickness dependent SRT.

In experimental points of view, the X-ray magnetic circular dichroism (XMCD) is a powerful tool to study the magnetic materials since one can directly extract magnetic information of specific element. Here, the spin and orbital sum rules play an essential role [39, 40] since the interpretation of experimental results is based on these sum rules. Nonetheless, it is rather rare to see studies for the general validity of the sum rule which is based on atomic model although one can find huge experimental data utilizing XMCD technique. Here, we have calculated X-ray absorption spectroscopy (XAS) and X-ray magnetic circular dichroism (XMCD) of Fe/Ni films using the *ab initio* method.

In this dissertation, various magnetic properties of thin films due to strain effect will be discussed using the full-potential linearized augmented plane wave (FLAPW) method. As mentioned above, the magnetic anisotropy energy (MAE) is very important quantity in magnetic device application. The MAE is divided into two parts, such as shape anisotropy and magnetocrystalline anisotropy (MCA). The shape anisotropy is originated from the magnetic dipole-dipole interaction and the MCA can be explained by spin-orbit coupling term. The X-ray magnetic circular dichroism (XMCD) is the most widely used to investigate the magnetic materials because XMCD can detect spin magnetic moment and orbital magnetic moment in individual atom. Therefore, the background theory of MAE and XMCD are discussed in chapter 2.

To investigate the magnetism of materials, many numerical methods have been used. Among these methods, the full-potential linearized augmented plane wave (FLAPW) method is very widely accepted due to the high precision.

FLAPW method is based on the density functional theory (DFT), and the DFT includes kinetic energy, potential energy, and exchange energy terms. To deal with exchange energy term, several approximation methods have been used, such as local density approximation (LDA) and generalized gradient approximation (GGA). Comparing LDA and GGA methods, the GGA method serves better accuracy than LDA method in 3d transition metal. The details will be reviewed in chapter 3. In chapter 4, the numerical results are discussed.



# Chapter 2 Basic Theory

## 2.1 Magnetic Anisotropy Energy

### 2.1.1 Introduction

In ferromagnetic materials, the exchange interaction between electrons is the origin of spontaneous magnetization. If there exists no external interaction, the spontaneous magnetization can point to certain direction in the crystal i.e., the spontaneous magnetization lies in some preferred directions with respect to the crystalline axes or to the external shape of the body. This phenomenon is the magnetic anisotropy. Here, the direction of spontaneous magnetization is easy axis, and other axes are hard axis. For example, the direction of magnetization is [001] axis in bulk Fe, so [001], [010], and [100] axes are easy axis. The magnetic anisotropy energy (MAE) is defined as the difference in energy between the easy axis and hard axis.

The magnetic anisotropy arises from dipolar interaction (shape anisotropy) and spin-orbit coupling (magnetocrystalline anisotropy). The shape anisotropy always prefers in-plane magnetization in film structure. However, the magnetocrystalline anisotropy (MCA) does not show simple behaviors.

In this section, we will discuss physical origins of magnetic anisotropy. In section 2.1.2 we present the phenomenological description of magnetic anisotropy at macroscopic level. The magnetic anisotropy arising from the dipole-dipole interactions and from the spin-orbit coupling will be treated in section 2.1.3 and 2.1.4, respectively.

## 2.1.2 Phenomenology of Magnetic Anisotropy

The MAE depends on the orientation of the magnetization with respect to the crystalline axes of the ferromagnetic body, and with respect to its shape (shape anisotropy). Thus, the total MAE may be expressed as

$$E_{MAE} = E_{MCA} + E_{sh}, \quad (2.1)$$

where  $E_{MAE}$ ,  $E_{MCA}$ , and  $E_{sh}$  are total magnetic anisotropy energy, magnetocrystalline anisotropy energy and shape anisotropy energy, respectively. It is clear that the first term is an intrinsic contribution, whereas the second one is essentially of geometric character.

The simplest case of the MAE is uniaxial magnetic anisotropy. One can see details in reference [13]. The hexagonal cobalt has easy axis, parallel to the c-axis of the crystal at room temperature. In other words, the MAE is increases with  $\theta$ , the angle between the c-axis and the magnetization vector. We can express MAE as following:

$$E_{MCA} = K_{u1}\sin^2\theta + K_{u2}\sin^4\theta + K_{u3}\sin^6\theta + K_{u4}\sin^6\theta\cos 6\varphi + \dots, \quad (2.2)$$

and

$$E_{MCA} = \frac{1}{2}K_{u1}(1 - \cos 2\theta) + \frac{1}{8}K_{u2}(3 - 4\cos 2\theta + \cos 4\theta) \quad (2.3) \\ + \frac{1}{32}K_{u3}(10 - 15\cos 2\theta + 6\cos 4\theta - \cos 6\theta) + \dots$$

where  $\varphi$  is the azimuthal angle of the magnetization in the plane perpendicular

to the c-axis and the coefficients  $K_{nu}$  are anisotropy constants.

For cubic crystals such as Fe and Ni, the MCA is can be expressed in term of the direction cosines ( $\alpha_1, \alpha_2, \alpha_3$ ) of the magnetization vector with respect to the three cube edges. The usual expression for the anisotropy of cubic system is

$$E_{MCA} = K_1 (\alpha_1^2 \alpha_2^2 + \alpha_2^2 \alpha_3^2 + \alpha_3^2 \alpha_1^2) + K_2 \alpha_1^2 \alpha_2^2 \alpha_3^2 \quad (2.4)$$

$$+ K_3 (\alpha_1^2 \alpha_2^2 + \alpha_2^2 \alpha_3^2 + \alpha_3^2 \alpha_1^2) + \dots$$

The anisotropy constants of hcp Co, Fe, and Ni are given in Table 2-1. Combining the values in Table 2-1 and equations (2.3) and (2.4), we can see that hcp Co have easy axis parallel to the c-axis. Also, Fe and Ni have easy axis for [100] and [111], respectively.

	Co (hcp)	Fe (bcc)	Ni (fcc)
$K_1$ (erg.cm <sup>-3</sup> )	$4.53 \times 10^6$ (a)	$5.48 \times 10^5$ (b)	$-12.63 \times 10^5$ (c)
$K_2$ (erg.cm <sup>-3</sup> )	$1.44 \times 10^6$ (a)	$1.96 \times 10^3$ (b)	$5.78 \times 10^5$ (c)

Table 2-1. Anisotropy constants of Co (T=15°C) , Fe (T=20°C), and Ni (T=23 °C). (a) Ref [14], (b) Ref [15], (c) Ref [16].

### 2.1.3 Anisotropy Arising from Dipolar Interactions.

The dipole-dipole interaction has been discussed by Janse [5]. The expression of the dipole-dipole Hamiltonian is

$$H_{dip} = \frac{\mu_B^2}{2} \int \int dr dr' \frac{1}{|r-r'|^3} \times \left( (\hat{m}(r) \cdot \hat{m}(r')) - \frac{3[(r-r') \cdot \hat{m}(r)][(r-r') \cdot \hat{m}(r')]}{|r-r'|^2} \right) \quad (2.5)$$

Where  $\hat{m}(r)$  is the magnetization density operator, expressed in  $\mu_B$  unit volume. In 3d transition metals, the magnetization distribution is almost spherical, and can be replaced by the dipolar magnetic moments  $m_i$ , so that the dipolar energy can be written as

$$E_{dip} = \frac{\mu_B^2}{2} \sum_{i \neq j} \frac{1}{r_{ij}^3} \left( m_i \cdot m_j - \frac{3(r_{ij} \cdot m_i)(r_{ij} \cdot m_j)}{r_{ij}^2} \right) \quad (2.6)$$

Because all magnetic moments are parallel in ferromagnetic materials,  $E_{dip}$  is

$$E_{dip} = \frac{\mu_B^2}{2} \sum_{i \neq j} \frac{m_i m_j}{r_{ij}^3} (1 - 3\cos^2\theta_{ij}) \quad (2.7)$$

where  $\theta_{ij}$  is the angle between magnetization and the direction of the pair  $(i, j)$ . For a give pair the dipolar energy is minimum when the moments are parallel to direction of pair.

### Shape Anisotropy

Because  $\vec{H}_{dip}(i)$  at site  $i$  produced by all the other dipole moments, does not depend on their exact positions at the atomic level, so that one can replace the individual moments by the continuous magnetization distribution  $\vec{M}(r)$ . These considerations are accounted for Lorentz method. A spherical cavity of radius  $R$  centered at site  $i$ , and the moment distribution is approximated by the macroscopic magnetization density  $\vec{M}(r)$ . Since the cavity space is bound by volume and surface, we can define magnetic charges, volume charge and surface charges,  $\rho_M = -\nabla \cdot \vec{M}$ , and  $\sigma_M = \hat{n} \cdot \vec{M}$ . In case the magnetization is uniform, the surface magnetic charges only contribute. Thus,  $H_{dip}(i)$  can be written

$$\vec{H}_{dip}(i) = \vec{H}_{cav} + \vec{H}_L + \vec{H}_d \quad (2.8)$$

where  $H_{cav}$  is due to the dipoles inside the cavity,  $H_L = (4\pi/3)M$  (the Lorentz field) is the field created by charges at surface of the cavity, and  $H_d$  (the demagnetizing field) is due to the charges on the external surface. The magnetic energy of the shape anisotropy is given by

$$E_{sh} = -\frac{1}{2} \int_V dV \vec{M}(r) \cdot \vec{H}_{dip}(r) \quad (2.9)$$

For the ellipsoid sample and uniform demagnetising field, the shape anisotropy is expressed in terms of a demagnetising tensor,

$$\vec{H}_{dip} = -4\pi D \cdot \vec{M} \quad (2.10)$$

where  $D$  is a tensor of trace 1. Then, the shape anisotropy per unit volume is  $E_{sh} = K_{shape} \sin^2 \theta$ , and  $K_{shape} = -2\pi M_V^2$ , where  $M_V$  refer to volume magnetization. For a layered system such as thin films and multi-layer films, The shape anisotropy energy are  $E_{sh}^s = K_{sh}^s \sin^2 \theta$ , and  $K_{sh}^s \approx -2\pi M_V M_s$ , where  $M_s$  is surface magnetization. From this equations, we can know that the shape anisotropy energy show in-plane direction for surface always.

### 2.1.3 Anisotropy Arising from the Spin-Orbit Coupling

When the electron moves at a velocity  $\vec{v} = \vec{p}/m_e$  in the electrostatic field  $\vec{E}$  created by core electrons and protons, the electron feels the magnetic field  $\vec{B}$  according to special relativity theory, and the magnetic field can be written as

$$\vec{B} = -\frac{1}{c^2} \vec{v} \times \vec{E}. \quad (2.11)$$

Since the electron has a moment  $\vec{p}$ , the electron moving in electrostatic field feels the magnetic field

$$\vec{B} = -\frac{\vec{p}}{mc} \times \vec{E}. \quad (2.12)$$

Therefore, the corresponding interaction energy between spin of electron and magnetic field  $\vec{B}$  is

$$\begin{aligned}
H' &= -\frac{1}{2} \vec{\mu} \cdot \vec{B} = \frac{1}{2} \vec{\mu} \cdot \left( \frac{\vec{v}}{c} \times \vec{E} \right) \\
&= -\frac{1}{2} \frac{\vec{\mu}}{mc} \cdot (\vec{E} \times \vec{p})
\end{aligned} \tag{2.13}$$

Because the electrostatic field  $\vec{E}$  equal to  $-\frac{dV(r)}{dr} \frac{\vec{r}}{r}$ ,

$$H' = \frac{1}{2} \frac{1}{mc} \left[ \frac{1}{r} \frac{dV(r)}{dr} \right] (\vec{r} \times \vec{p}) \cdot \vec{\mu} \tag{2.14}$$

Using the  $\vec{\mu} = \left( \frac{e}{mc} \right) \vec{S}$  and  $\vec{r} \times \vec{p} = \vec{L}$ , we can replace  $H'$  following as,

$$H' = \frac{e}{2m^2c^2} \left[ \frac{1}{r} \frac{dV(r)}{dr} \right] \vec{L} \cdot \vec{S}. \tag{2.15}$$

Thus, we find the quantum mechanical operator of spin-orbit coupling,

$$H_{SOC} = \xi(r) \hat{L} \cdot \hat{S}, \tag{2.16}$$

$$\xi(r) = \frac{1}{4m^2c^2} \frac{1}{r} \frac{dV}{dr} \tag{2.17}$$

where  $\xi$  is the spin-orbit constant.

To calculate MCA, several methods are used. In the direct method, the MCA can be calculated by comparing the total energy between two systems, in-plane and out-of-plane magnetization for surface systems. However, the MCA has the value of several  $\mu eV$ . In most of sample, this value is hard to

distinguish from numerical error of total energy calculation. Another method is force theorem, but this method require very large computational power. According to ref [42], the calculations can be simplified by torque method, and the torque is written as,

$$T(\theta) = \sum_{occ.} \left\langle \psi_{i,k}^{so} \left| \frac{\partial H_{so}}{\partial \theta} \right| \psi_{i,k}^{so} \right\rangle, \quad (2.18)$$

where  $H_{so}$  is spin-orbit coupling Hamiltonian. If magnetization direction is  $\vec{n}(\theta, \phi)$ , the  $\vec{L} \cdot \vec{S}$  term can be expressed as,

$$\begin{aligned} \vec{L} \cdot \vec{S} = & s_n (l_z \cos \theta + \frac{1}{2} l_+ e^{-i\phi} \sin \theta + \frac{1}{2} l_- e^{i\phi} \sin \theta) \\ & + \frac{1}{2} s_+ \left( -l_z \sin \theta - l_+ e^{-i\phi} \sin^2 \frac{\theta}{2} + l_- e^{i\phi} \cos^2 \frac{\theta}{2} \right) \\ & + \frac{1}{2} s_- \left( -l_z \sin \theta + l_+ e^{-i\phi} \cos^2 \frac{\theta}{2} - l_- e^{i\phi} \sin^2 \frac{\theta}{2} \right) \end{aligned} \quad (2.19)$$

In this equation, we can know that the MCA does not depend on the crystal symmetry.

## 2.2 X-ray Magnetic Circular Dichroism (XMCD)

The magnetic properties of the 3d transition metals are mainly determined by their d valence electrons [18-20]. The properties of 3d-electrons are best probed in an X-ray absorption experiment by excitation of 2p core electrons to unfilled 3d states as illustrated by a simple one-electron picture [17]. According to the one electron approach, the electron is excited from the spin-orbit split  $2p_{3/2}$  and  $2p_{1/2}$  levels to empty d valence states. The origin of circular x-ray dichroism at the  $L_{2,3}$  edges of 3d transition metals is illustrated by two-step model proposed by Stöhr [5]. In the first step, right(+) or left(-) circularly polarized photons excite the spin-polarized electrons in p shell. In spin-orbit split levels,  $p_{3/2}$  ( $L_3$ , 1+s) and  $p_{1/2}$  ( $L_2$ , 1-s) levels have opposite spin-orbit coupling, so that the spin polarization will be opposite sign. Then, each circularly polarized photons can excite spin up or spin down electrons each other.

In second step, the magnetic properties can be analyzed. As shown in Fig. 2-1(a), the XMCD intensities, A ( $L_3$  edge) and B( $L_2$  edge), can determine the spin moment quantitatively using the spin sum rule,  $A-2B$ , and orbital momentum can be measured by orbital sum rule,  $A+B$ , as shown in Fig 2-1 (b). The details of XMCD spectroscopy is in ref [17].

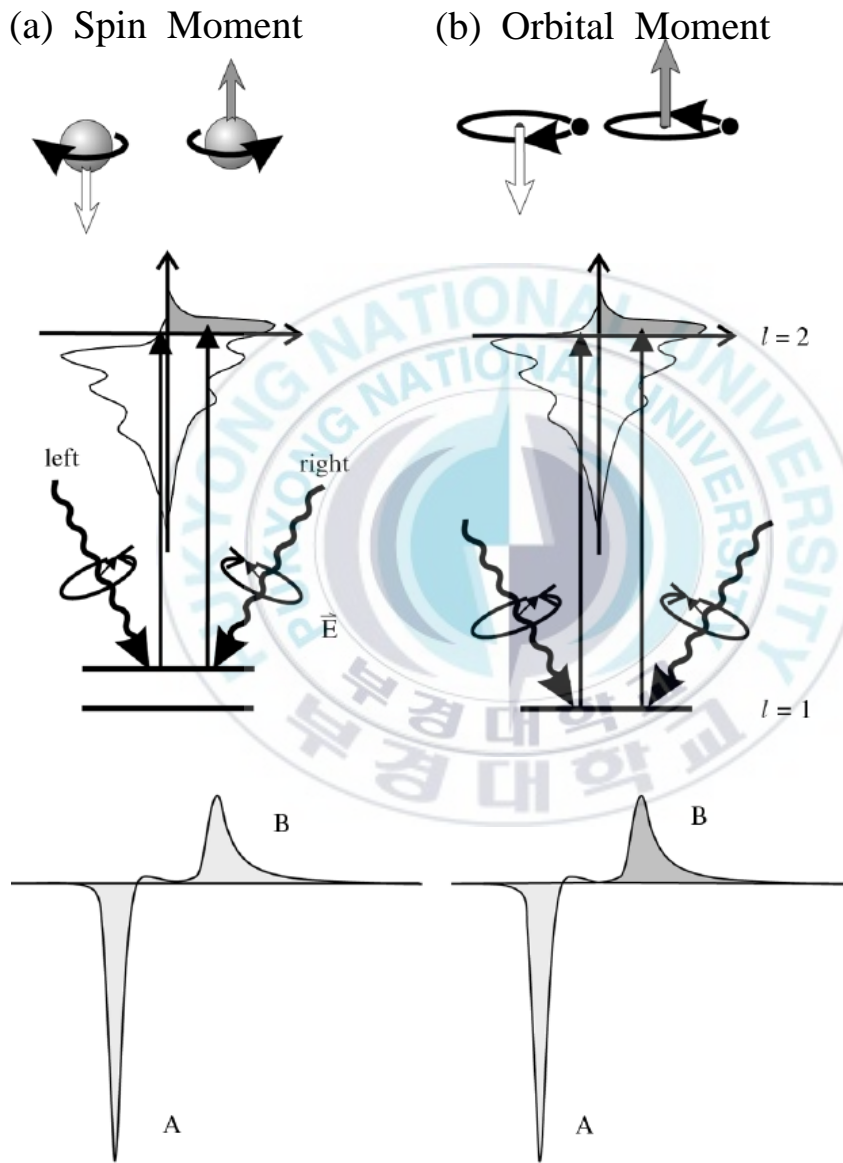


Fig 2-1. XMCD illustrated in a one-electron model. (a) is spin moment and (b) is orbital moment. [from reference 17].

# Chapter 3 FLAPW Method

## 3.1 The Density Functional Theory

### 3.1.1 The Density Functional Theory

The FLAPW method bases on density-functional theory (DFT), called Hohenberg-Kohn-Sham or Kohn-Sham equation[29, 30]. In the DFT, the total energy of a periodic solid is a functional of the atomic positions and the electron density, and consists of three parts, kinetic, potential and exchange correlation terms. In this section will review the density functional theory.

To explore the physical properties of real materials, quantum mechanical method is required and also has to solve many body problem. In many body problem, there are huge number of interaction among electrons and ions such electron-electron, electron-ion, and ion-ion interaction. The Born-Oppenheimer approximation [31] assumes that the motion of nuclei is so slow compared with electrons that the motion of nuclei can be neglected. This implies that the position of nuclei is fixed and the electronic structure is obtained for a specific atomic geometry.

Let us assume the system having N interacting electrons. The system is influenced under the external potential and the Coulomb repulsion which is electron-electron interaction, the Hamiltonian can be written as follows.

$$H = T + V + U, \quad (3.1)$$

where T is kinetic energy operator,

$$T = -\frac{\hbar^2}{2m} \sum_i \nabla_i^2, \quad (3.2)$$

and the external potential,  $V$ , is expressed by two terms due to external field and fixed ions.

$$V = \sum_i V_{field}(r_i) + \sum_{ij} V_{ion}(r_i - R_j), \quad (3.3)$$

where  $r_i$  and  $R_j$  indicate the position of  $i$ -th electron and  $j$ -th ion, respectively. The Coulomb repulsion interaction (electron-electron interaction) is follows:

$$U = \sum_{i \neq j} \frac{e^2}{|r_i - r_j|} \quad (3.4)$$

Now, we will reconstruct this Hamiltonian using the electron density,  $\rho(r)$ . The electron density is given by:

$$\rho(r) = \sum_i n_i |\psi_i(r)|^2 \quad (3.5)$$

where  $\psi_i$  is the single-particle wave function and  $n_i$  is the number of electrons in state  $i$ . Kohn and Sham expressed the ground state energy in the static potential  $V_{ext}$ :

$$E[\rho(r)] = \int V_{ext} \rho(r) dr + \frac{1}{2} \int \int \frac{\rho(r)\rho(r')}{|r-r'|} dr dr' + G[\rho(r)], \quad (3.6)$$

$$G[\rho(r)] = T[\rho(r)] + E_{xc}[\rho(r)] \quad (3.7)$$

where  $\int \int \frac{\rho(r)\rho(r')}{|r-r'|} dr dr'$  is Hartree energy,  $T[\rho(r)]$  refer to kinetic energy, and  $E_{xc}[\rho(r)]$  means exchange-correlation energy. Applying variational principle to equation (3.6),

$$\int \delta\rho(r) \left( \varphi(r) + \frac{\delta T[\rho(r)]}{\delta\rho(r)} + \mu_{xc}[\rho(r)] \right) dr = 0 \quad (3.8)$$

here,

$$\varphi(r) = V_{ext}(r) + \int \frac{\rho(r')}{|r-r'|} dr' \quad (3.9)$$

and

$$\mu_{ex}[\rho(r)] = \partial E_{xc}[\rho(r)] / \partial\rho(r) \quad (3.10)$$

The equation (3.8) means that system is under given potential  $\varphi(r) + \mu_{xc}[\rho(r)]$ .

Therefore, one can obtain simple the one-particle Schrödinger equation

$$\left[ -\frac{\hbar^2}{2m} \nabla^2 + V_{eff}(r) \right] \psi_i(r) = \varepsilon_i \psi_i(r), \quad (3.11)$$

where,  $V_{eff}(r) = \varphi(r) + \mu_{ex}[\rho(r)]$ . Equation (3.11) is the Kohn-Sham equations and  $\psi_i(r)$  is an orthonormal set. Also, the exchange-correlation potential (interaction and energy) should be explained by approximation method.

### 3.1.2 Spin-polarized density functional theory

To deal with magnetic materials, the density functional theory has to include the spin polarized electrons and magnetization is not zero. Because the exchange correlation potential of the Kohn-Sham equation have electron density terms,  $\rho(r)$ , the electron density divide into spin-up and spin-down expressed as  $\rho(r) = \rho(r)_\uparrow + \rho(r)_\downarrow$ . Also, the magnetization density,  $\sigma = \rho_\uparrow - \rho_\downarrow$  is important value. In magnetic system, the magnetization density has spin-up or spin-down. Therefore, the spin-polarized Kohn-Sham equations are

$$\left[-\frac{\hbar^2}{2m}\nabla^2 + V_{eff}^\sigma(r)\right]\psi_i^\sigma(r) = \varepsilon_i^\sigma\psi_i^\sigma(r), \quad (3.12)$$

where,  $\sigma$  is spin-up ( $\uparrow$ , or majority) or spin-down ( $\downarrow$ , or minority), and

$$V_{eff}^\sigma(r) = V_C(r) + \mu_{xc}^\sigma[\rho(r), \sigma(r)]. \quad (3.13)$$

In equation (3.12), the wave function  $\psi_i^\sigma$  is single-particle wave function and can have two spin state, spin-up and spin-down.

### 3.1.3 Approximation method for exchange-correlation

The density functional formalism has the exchange correlation term. To obtain exact solution of systems, the exchange correlation energy  $E_{xc}$  is essential, but explicit form of this functional has not been found yet. Thus, approximations should be used. Mostly used approximation methods are the local density

approximation (LDA) and the generalized gradient approximation (GGA).

### ***Local density approximation (LDA)***

It is the underlying idea of LDA that the exchange correlation energy depend only on the local electron density of each volume element  $dr$ .

$$E_{xc}[\rho] \approx \int \rho(r) \varepsilon_{xc}[\rho(r)] dr, \quad (3.14)$$

where,  $\varepsilon_{xc}[\rho]$  is the exchange correlation energy per electron of a homogeneous electron gas with the same electron and magnetization density.

### ***Generalized gradient approximation (GGA)***

The generalized gradient approximation (GGA) have improved the description of total energies, ionization energies, and electron affinities of atoms, atomization energies of molecules [32, 33, 34] and some solid state properties [35, 36, 37, 38]. The GGA is written as:

$$E_{xc}^{GGA}[\rho] = \int \rho(r) \varepsilon_{xc}^{GGA}[\rho(r), \nabla \rho(r)] dr \quad (3.15)$$

As shown above, GGA depends on locally on the electronic density  $\rho(r)$  and its gradient. This method means non-homogeneous electron gas system.

## 3.2 The Thin Film Version FLAPW and Basis-set

### 3.2.1 Introduction.

In this section we will review the full-potential linear augmented plane wave (FLAPW) method [21-23]. The FLAPW method to solve the density functional equation for crystalline solid is presently one of the most accurate electronic structure calculation methods. This method originates from the augmented plane wave (APW) method introduced by Slater [24]. Within the APW approach, space is divided into spheres centered at each atom site, called muffin-tins (MT), and the remaining interstitial region. Inside the muffin-tins the potential is approximated by a spherically symmetric shape, and in many implementations the interstitial potential is set to a constant. Since the basis functions of APW method are energy dependent and the eigenvalue problem nonlinear, APW method is computationally very demanding. To avoid the problems of APW method, the linearized APW (LAPW) method is introduced [25, 26]. The energy dependence is removed by selection a fixed set of suitable muffin-tin radial functions and their energy derivatives. The APW and LAPW method regard potential, actually effective potential, in MT region as constant. However, these assumptions are not suitable in several problems such as magnetic materials, because spherically symmetry breaking should be considered in magnetic materials. Therefore, the full-potential LAPW (FLAPW) method is introduced, and has no shape approximation for the charge density and the potential. Also, the core electrons are treated full relativistically and the valence electrons are treated semi-relativistically [27, 28].

### 3.2.2 The FLAPW method and Basis-set

The films have only the 2-dimensional symmetry parallel to the surface and there is a number of atomic layers surrounded by vacuum between  $\pm D/2$  and  $\pm \tilde{D}/2$  (see fig. 3-1.) in z-direction. In the thin film version FLAPW method, real space is divided into three regions, the muffin-tins, the interstitial and the vacuum region show as Fig. 3-1. In the spherical region, the basis functions are products of radial functions and spherical harmonics, in the interstitial region plane waves are used. In the vacuum region, the wave functions are products of two-dimensional (2D) plane waves and z-dependent functions which are solutions of the one-dimensional Schrödinger equation for z-axis. For film geometry, the wave functions are given by

$$\psi_i(r, k_{\parallel}) = \sum_j c_{ij} \phi(r, K_j); \quad K_j = k_{\parallel} + G_j, \quad (3.16)$$

where  $k_{\parallel}$  is an arbitrary vector of the two dimensional Brillouin Zone (BZ) and  $G_j$  is a three dimensional reciprocal lattice vector. The basis functions are:

$$\phi(r, K_j) = \begin{cases} \Omega^{-1/2} e^{iK_j r} & \text{interstitial} \\ \sum_{lm} [A_{lm}^{\alpha}(K_j) u_l(E_l^{\alpha}, r_{\alpha}) + B_{lm}^{\alpha}(K_j) \dot{u}_l(E_l^{\alpha}, r_{\alpha})] Y_{lm}(\hat{r}_a) & \text{sphere} \\ \sum_q [A_q(K_j) u_{kq}(E_{\nu}, z) + B_q(K_j) \dot{u}_{kq}(E_{\nu}, z)] e^{i(k_{\parallel} + K_{\parallel q})r} & \text{vacuum} \end{cases} \quad (3.17)$$

In the muffin-tin region two radial wave functions are  $u_l$  and  $\dot{u}_l$ , where  $u_l$  is the solutions of the radial Schrödinger equation solved at a fixed energy,  $E_l$ ,

$$\frac{1}{2r} \frac{d^2}{dr^2} [ru_l(r)] - \frac{l(l+1)}{2r^2} u_l(r) + [E_l - V_{eff}(r)] u_l(r) + h_r u_l(r) = 0, \quad (3.18)$$

and  $\dot{u}_l$  is derivatives of  $u_l$ . Here we assume that  $h = m = e = 1$ . The  $Y_{lm}$  are spherical harmonics and the coefficients  $A_{lm}^\alpha$  and  $B_{lm}^\alpha$  are determined by the requirement that the plane waves be continuous in value, as be their radial derivative, at the atomic spheres. The  $\Omega$  is the volume per unit cell from  $-\tilde{D}/2$  to  $+\tilde{D}/2$ . In the vacuum region the wave functions,  $u_{kq}$  can be obtained from one dimensional Schrödinger equation in z-direction.

$$\left[ -\frac{1}{2} \frac{\partial^2}{\partial z^2} + V_{eff}(z) - (E_\nu - K_{\parallel q}) \right] u_{kq}(E_\nu, z) = 0, \quad (3.19)$$

where  $V_{eff}(z)$  is the planar average of the effective potential perpendicular to the surface,  $E_\nu$  are fixed energy parameters for the vacuum region, and  $K_{\parallel q}$  refer to 2D reciprocal lattice vectors of the lattice parallel to the surface.

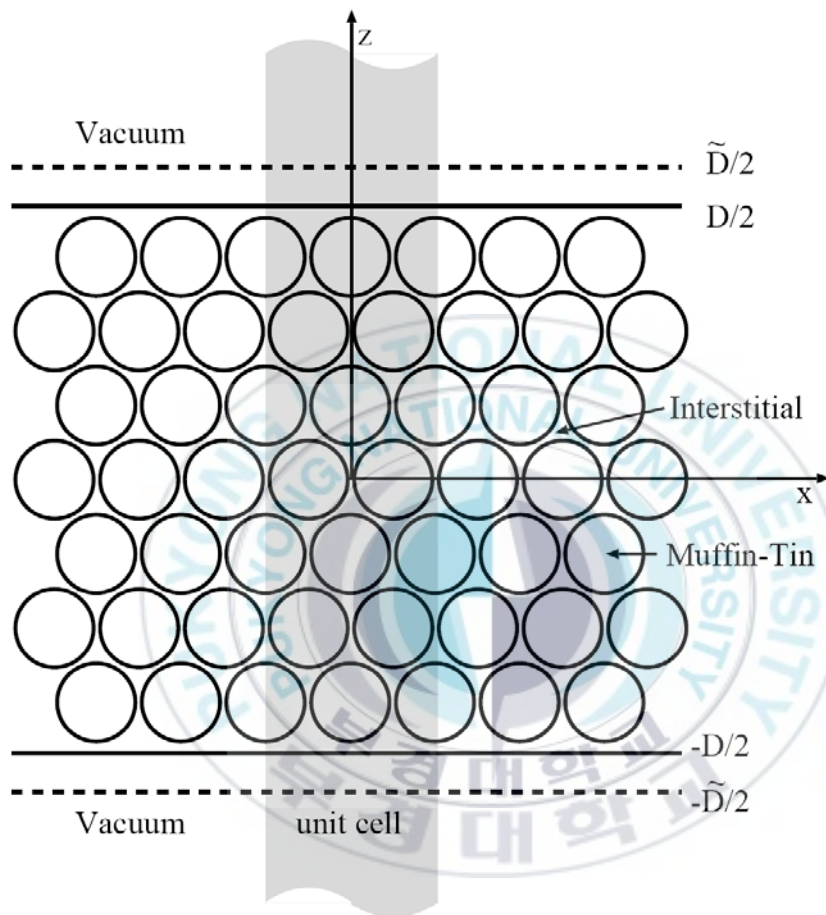


Fig. 3-1. Geometry for a film calculation.

# Chapter 4. Computational Results

## 4.1 Numerical Method.

The thin film version of all-electron full potential linearized augmented plane wave (FLAPW) method [41-42] was used to explore this issues. Therefore, there is no shape approximation in charge, potential and wave function expansion. We treat the core electrons fully relativistically. The generalized gradient approximation (GGA) [43] was adopted to describe the exchange correlation interaction. Spherical harmonics with a maximum angular momentum quantum number of  $l_{\max} = 8$  were used for all the expansions in the muffin-tin region. In the FLAPW calculations, energy cutoffs of 255 Ry for the charge and potential, and 13.7 Ry for the bases were chosen in the interstitial region. We used 400 k-points for entire calculations in the irreducible two-dimensional Brillouin zone to evaluate integrals in the reciprocal space and employed 2.2 a.u. for muffin-tin (MT) radius of all atoms. Because the main issue is to study the magnetic properties depending on Fe and Ni thickness. Therefore, we have considered four different systems. The Fe coverage is varied from 0.5 to 2.5 ML and the ultrathin Fe film is assumed to be grown on 5 and 7ML Ni under-layer. Moreover, the Fe/Ni film is supposed to grow with Cu(001) lattice constant and Ni(001) lattice constant, respectively. Also, we assume that Ni and Fe have fcc centered cubic structure. With this approach, we will be able to understand the effect of strain on the SRT. As remarked earlier, the magnetic anisotropy is significantly dependent on the change of electronic structure. Consequently, it is of necessary to obtain optimized atomic structure and this has been achieved through total energy and force minimization procedures

## 4.2 Numerical Results and Discussion

### 4.2.1 Structural Feature

We have calculated the optimized atomic position and vertical distance using the total energy and force minimization procedure. In Figure 4-1, the Ni at the interface between Ni and Fe adlayer is represented by  $Ni_s$  and the subsurface layer is denoted by  $Ni_{s-1}$ . The  $Fe_i$  stands for  $i$ -th adlayer counted from the interface. Also,  $D_{Ni}$  and  $D_i$  mean calculated vertical distance between two neighbor atoms as in Fig 4-1 and the values are given in Table 4-1. One can clearly see that the optimized atomic structures are sensitive to the strain effect. For instance, the vertical positions are always higher in the presence of strain compared to those in pseudomorphic growth and the interlayer distance is also changed. Nonetheless, we have realized that the strain has minimal effect on the magnetic moments of Fe and Ni atoms because the calculated magnetic moments are almost intact. This could be understandable because the magnetic moment is simply the difference between majority and minority spin electrons below Fermi level. The intensive discussions about magnetic moment and density of states (DOS) features will be discussed in next two sections. However, the physical property of magnetic anisotropy shows completely different behaviors. In Figs. 4-2(a) and (b), the experimentally observed thickness dependent magnetic anisotropy is presented. The theoretically obtained results are shown in Fig. 4-2(c). The solid symbols mean in-plane magnetization, while the open symbols denote perpendicular magnetization to the film surface. In Fig. 4-2(c), the thickness dependent magnetic anisotropy for pseudomorphic growth is indicated by open square which means perpendicular magnetization. In the presence of strain effect (denoted by circles), it has been achieved that the magnetic

anisotropy shows more or less oscillatory behaviors. As discussed earlier, the strain has physically no effect on the magnetic moment, but the strain influence on the magnetic anisotropy plays an essential role. The feature stems from that the wave function characters of both occupied and unoccupied states enter into the determination of magnetization direction, whereas the magnetic moment is simply the difference in the spin split states below the Fermi level.

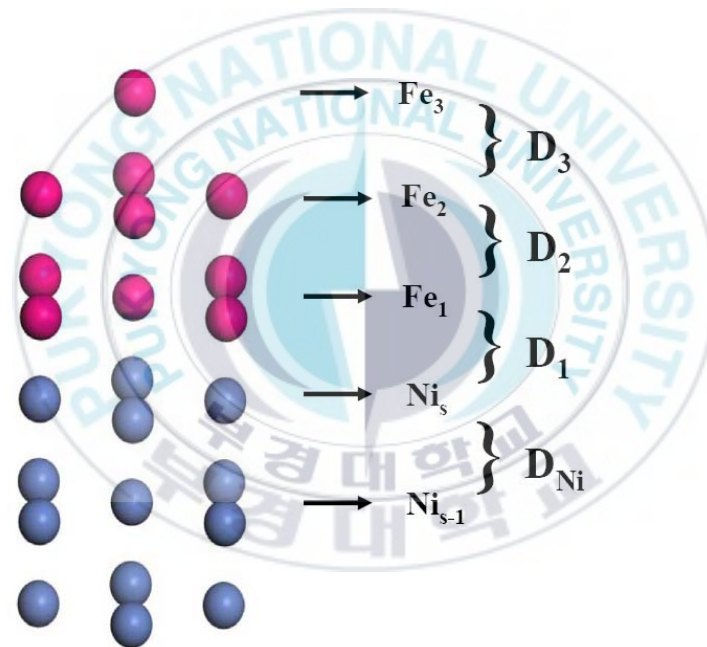


**Fig. 4-1.** Schematic side view of the Fe/Ni ultra-thin film structure.

(a) Fe/Ni(7ML)/Cu

Fe coverage	0.5ML	1ML	1.5ML	2ML	2.5ML
D <sub>3</sub>					3.02
D <sub>2</sub>			3.029	3.502	3.396
D <sub>1</sub>	2.783	3.283	3.258	3.311	3.179
D <sub>Ni</sub>	3.358	3.283	3.251	3.243	3.214

(b) Fe/Ni(7ML)

Fe coverage	0.5ML	1ML	1.5ML	2ML	2.5ML
D <sub>3</sub>					3.240
D <sub>2</sub>			3.240	3.749	3.560
D <sub>1</sub>	2.918	3.509	3.358	3.589	3.348
D <sub>Ni</sub>	3.507	3.447	3.397	3.447	3.337

(c) Fe/Ni(5ML)/Cu

Fe coverage	0.5ML	1ML	1.5ML	2ML	2.5ML
D <sub>3</sub>					3.010
D <sub>2</sub>			3.085	3.500	3.402
D <sub>1</sub>	2.793	3.345	3.195	3.295	3.215
D <sub>Ni</sub>	3.369	3.326	3.278	3.276	3.240

(d) Fe/Ni(5ML)

Fe coverage	0.5ML	1ML	1.5ML	2ML	2.5ML
D <sub>3</sub>					3.310
D <sub>2</sub>			3.270	3.639	3.578
D <sub>1</sub>	2.927	3.447	3.397	3.467	3.357
D <sub>Ni</sub>	3.466	3.376	3.376	3.376	3.366

Table 4-1. Calculated vertical atomic distance in atomic unit.

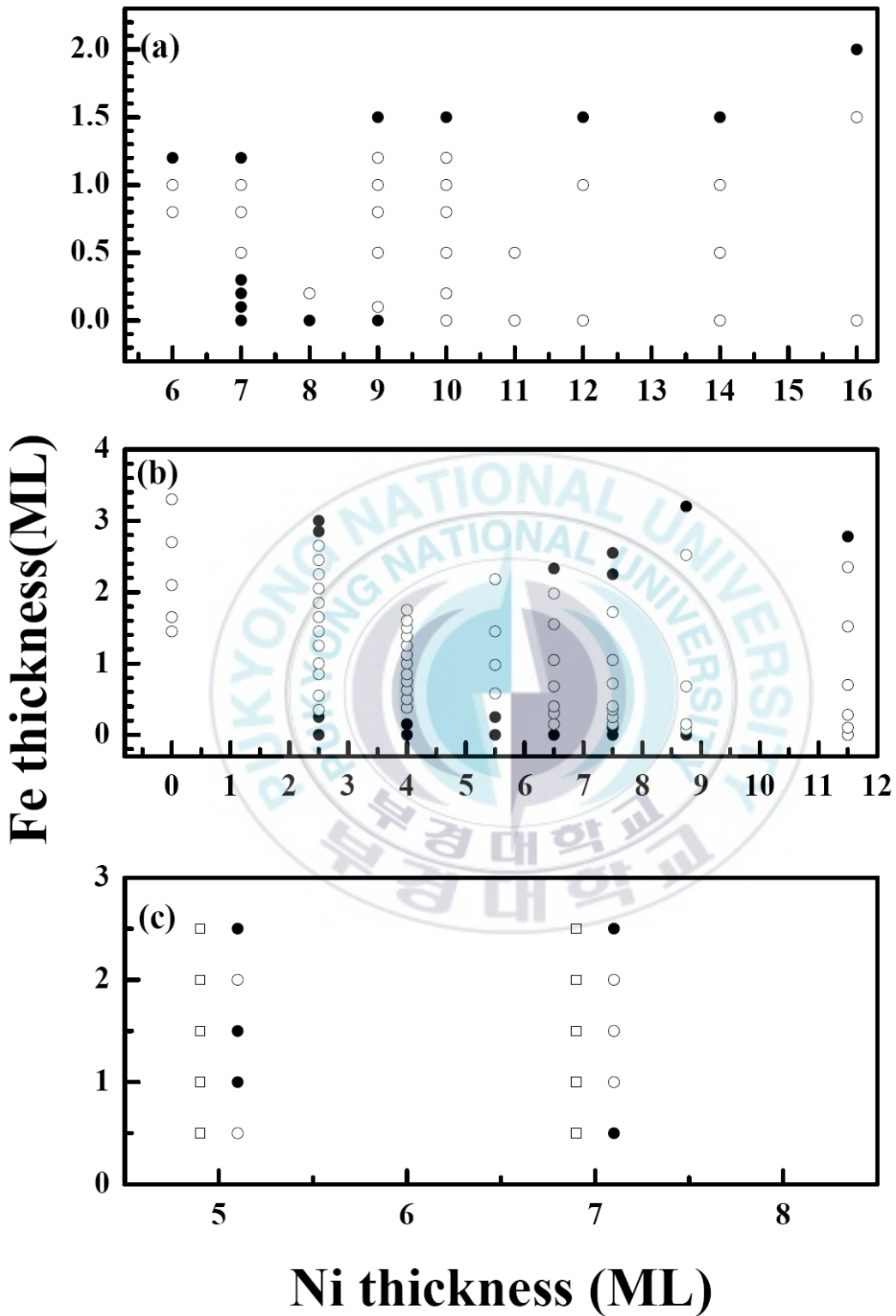


**Fig. 4-2.** Magnetic anisotropy energy phase of Fe/Ni/Cu ultra thin films. (a) and (b) are experimental results and (c) indicates calculated result.

## 4.2.2 Magnetic Moment

In Table 4-2, we show the calculated magnetic moments of Ni and Fe atoms for 5 and 7 ML Ni thicknesses if the film pseudomorphically grows with Cu(001) lattice constant. One can see that the magnetic moment of Fe at the top layer is greatly enhanced compared with that of bulk Fe atom and this is a typical surface enhancement. For Ni, the interface ( $Ni_S$ ) atom has the largest magnetic moment when the Fe coverage is 0.5 ML. With increasing Fe thickness, the interface Ni magnetic moment decreases rapidly. Note that the  $Ni_{S-1}$  for 0.5ML and  $Ni_S$  for 1.5ML thicknesses have two different values. This is due to atomic structure effect because we have two inequivalent atoms in a unit cell. Thus, one can easily note that the  $Ni_{S-1}$  in 0.5 ML and  $Ni_S$  in 1.5ML will encounter different environment in the presence of 0.5 ML coverage Fe adlayer. Thus, these two Ni atoms have different magnetic exchange interaction with Fe. For deeper layers, we have found no significant changes. This implies that the hybridization effect propagates definitely at least into the first two or three Ni layers and it is sizable. We have obtained similar results for 7 ML of Ni underlayer thickness. Overall, the calculated magnetic moments display almost the same behaviors and this is understandable since the magnetic exchange interaction will not be significantly altered even if another Ni layer exists in deep region. In Table 4-3, we present the results provided that the Fe/Ni film grows with the Ni(001) lattice constant in which the strain effect of 2–3% is considered. Comparing both cases, we have realized that the magnetic moments are rather insensitive to the strain effect although the small variations are observed.

(a)

	0.5 ML	1 ML	1.5 ML	2 ML	2.5 ML
Fe <sub>3</sub>					2.91
Fe <sub>2</sub>			2.97	2.85	2.60
Fe <sub>1</sub>	3.14	2.866	2.66	2.65	2.55, 2.64
Ni <sub>s</sub>	0.75	0.674	0.61, 0.69	0.65	0.68

(b)

	0.5 ML	1 ML	1.5 ML	2 ML	2.5 ML
Fe <sub>3</sub>					2.92
Fe <sub>2</sub>			2.95	2.84	2.60
Fe <sub>1</sub>	3.14	2.89	2.67	2.66	2.54, 2.62
Ni <sub>s</sub>	0.75	0.68	0.61	0.65	0.68

**Table 4-2.** Calculated magnetic moments (in  $\mu_B$ ) of Ni and Fe atoms for (a) 5 and (b) 7 ML Ni thickness with Cu(001) lattice constant

(a)

	0.5 ML	1 ML	1.5 ML	2 ML	2.5 ML
Fe <sub>3</sub>					3.00
Fe <sub>2</sub>			3.00	2.78	2.55
Fe <sub>1</sub>	3.14	2.86	2.62	2.64	2.53, 2.93
Ni <sub>s</sub>	0.74	0.66	0.63, 0.60	0.63	0.65

(b)

	0.5 ML	1 ML	1.5 ML	2 ML	2.5 ML
Fe <sub>3</sub>					2.98
Fe <sub>2</sub>			2.99	2.79	2.53
Fe <sub>1</sub>	3.15	2.87	2.61	2.69	2.52, 2.59
Ni <sub>s</sub>	0.75	0.66	0.65 0.60	0.63	0.66

**Table 4-3.** Calculated magnetic moments (in  $\mu_B$ ) of Ni and Fe atoms for (a) 5 and (b) 7 ML Ni thickness with Ni(001) lattice constant

### 4.2.3 Density of State

In this section, we show the density of states (DOS) features with two different lattice parameters, *i.e.* Cu(001) and Ni(001) lattice constants. The dotted and solid lines are for Cu(001) and Ni(001) lattice constants, respectively. In Figs. 4-3(a) and (b) the DOS of interface Ni atom for 5 and 7 ML of Ni underlayer thickness with 0.5ML Fe adlayer. One can see that the interface Ni DOS has almost the same feature with two different Ni underlayer thicknesses. This is quite natural since the interface Ni atom is insensitive to the presence of bottom layers and only few majority spin states are found near the Fermi level which means close to half metallic character. In Figs. 4-4(a) and (b), we present DOS of Fe atom for 5 and 7 ML of Ni surface, respectively. Once again, the DOS shows almost the same feature regardless of the Ni underlayer thickness and the strain effect. Interestingly, the 0.5ML Fe adlayer has a half metallic state and the band width is very narrow compared with that of Ni atom. This narrowing is due to the lack of neighboring atom. Even with increasing Fe adlayer thickness, we have found no physically meaningful changes for the DOS of interface Ni atom (not shown here). In Figs. 4-5(a) and (b), we show the DOS of Fe<sub>2</sub> and Fe<sub>1</sub> atoms for 1.5 ML Fe coverage, respectively. The DOS of top Fe layer (Fe<sub>2</sub> which is corresponding to 0.5ML coverage part) has still a half metallic feature although little broadening of band width is observed. The DOS of Fe<sub>1</sub> which is adjacent to the Ni surface has different behavior from that of top Fe layer. The half metallic feature vanishes and one can see more broadening. This is definitely originated from the hybridization with neighboring Fe atom in the same layer. For other systems the spectral shapes of DOS have changed, nonetheless the essential feature for magnetic moment almost remains the same and the half metallic state for top Fe layer is always found resulting in large magnetic moment.

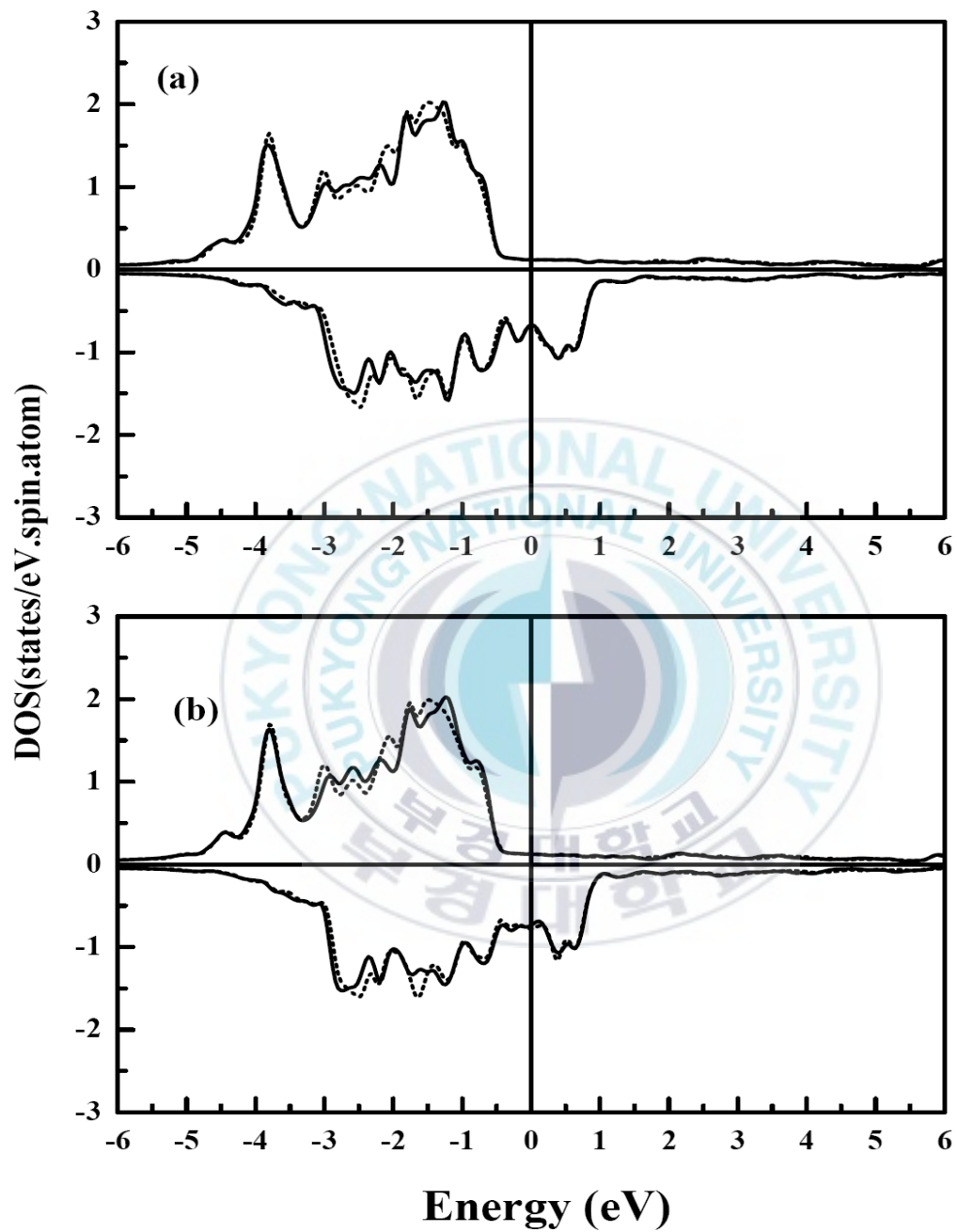


**Fig. 4-3.** DOS of interface Ni atoms with (a) 5ML Ni underlayer thickness, (b) 7ML Ni underlayer thickness. Both cases are for 0.5 ML Fe adlayer.

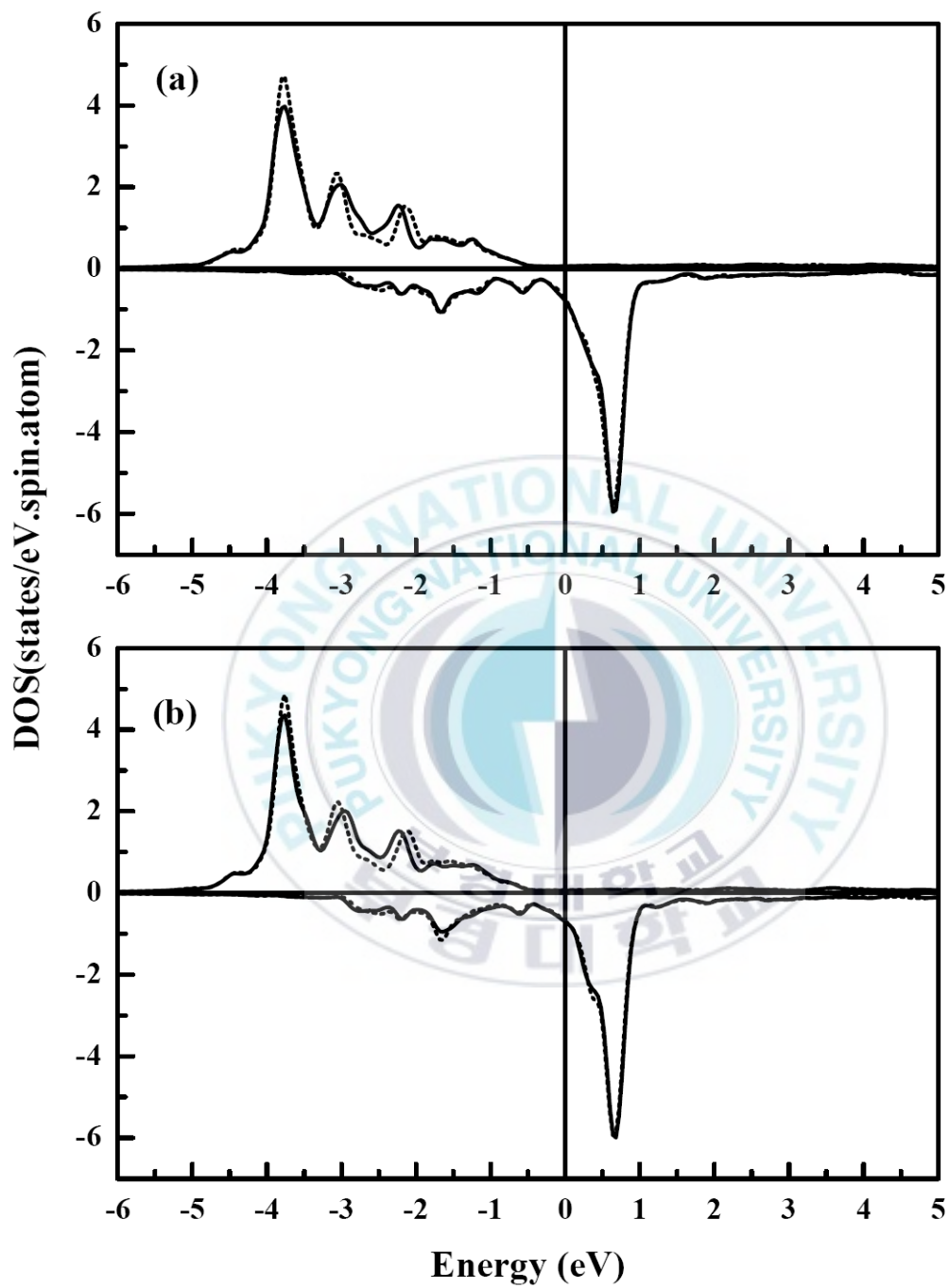


**Fig. 4-4.** DOS of Fe atom with 0.5 ML coverage with (a) 5ML Ni underlayer thickness, (b) 7ML Ni underlayer thickness.

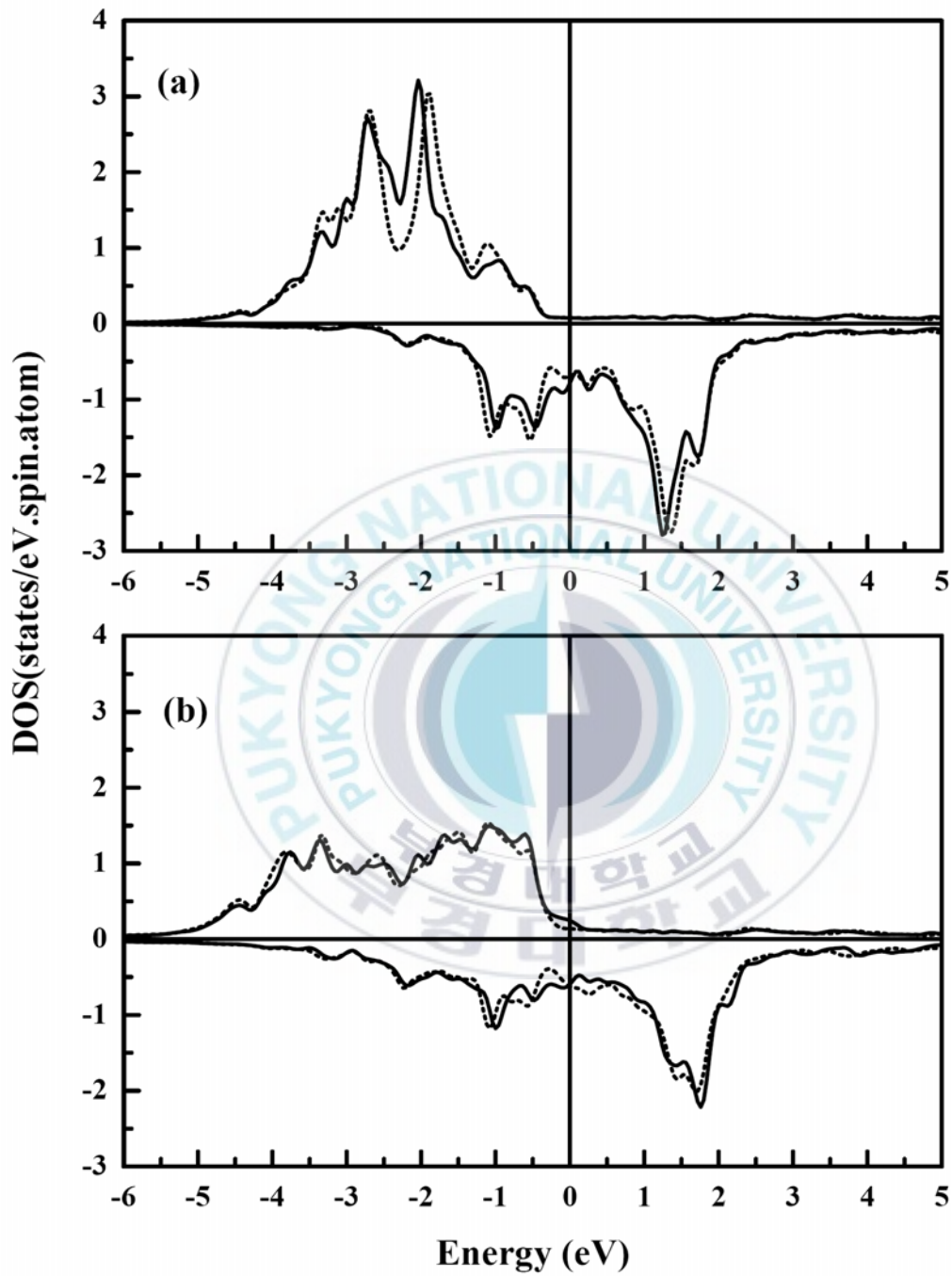


**Fig. 4-5.** DOS of Fe for 1.5ML Fe coverage with (a) top Fe layer which corresponds to 0.5ML coverage part, (b) Fe layer which corresponds to 1ML part.

## 4.2.4 Magnetic Anisotropy Energy

Recently, the thickness dependent magnetic anisotropy of Fe/Ni/Cu(001) has been explored, but these two experimental data show somewhat different results. For instance, Abe et al. have shown that the Fe/Ni has a perpendicular magnetization when the Fe adlayer thickness is about 0.5 - 1 ML level with 7 ML thickness of Ni underlayer otherwise an in-plane magnetization has been found [10]. On the other hand, Thamankar et al. have presented that the perpendicular magnetization appears up to 2 ML Fe thickness [11]. Several factors like different interface structures due to different growing condition, strain effect, adlayer effect can cause such a disparity. Nevertheless, the physical origin is not clearly revealed. In theoretical view point, the magnetocrystalline anisotropy (MCA) stems from the spin-orbit interaction which is a relativistic effect. Therefore, one needs to employ very accurate method to consider such a relativistic quantity. Among various numerical methods to calculate magnetic anisotropy energy (MAE), it has been known that the torque method is highly reliable and accurate even with fewer k-points. Thus, in our calculations we employ this method [42]. The calculated magnetic moments and DOS studies have revealed that the strain effect and thickness dependence seem minimally effective. The spin magnetic moment is simply the difference between occupied majority and minority spin electrons and this has nothing to do with the wave function character. Nonetheless, the MCA can have completely different behaviors since it is substantially dependent on the wave function features. We thus theoretically explored the magnetic anisotropy of Fe/Ni/Cu(001) thin films. Four different structures have been considered, *i.e.* Fe/Ni for 5 and 7 ML thicknesses of Ni underlayer with two different lattice parameters. We have assumed that the Fe/Ni films grow with Cu(001) and Ni(001) lattice constants in lateral direction,

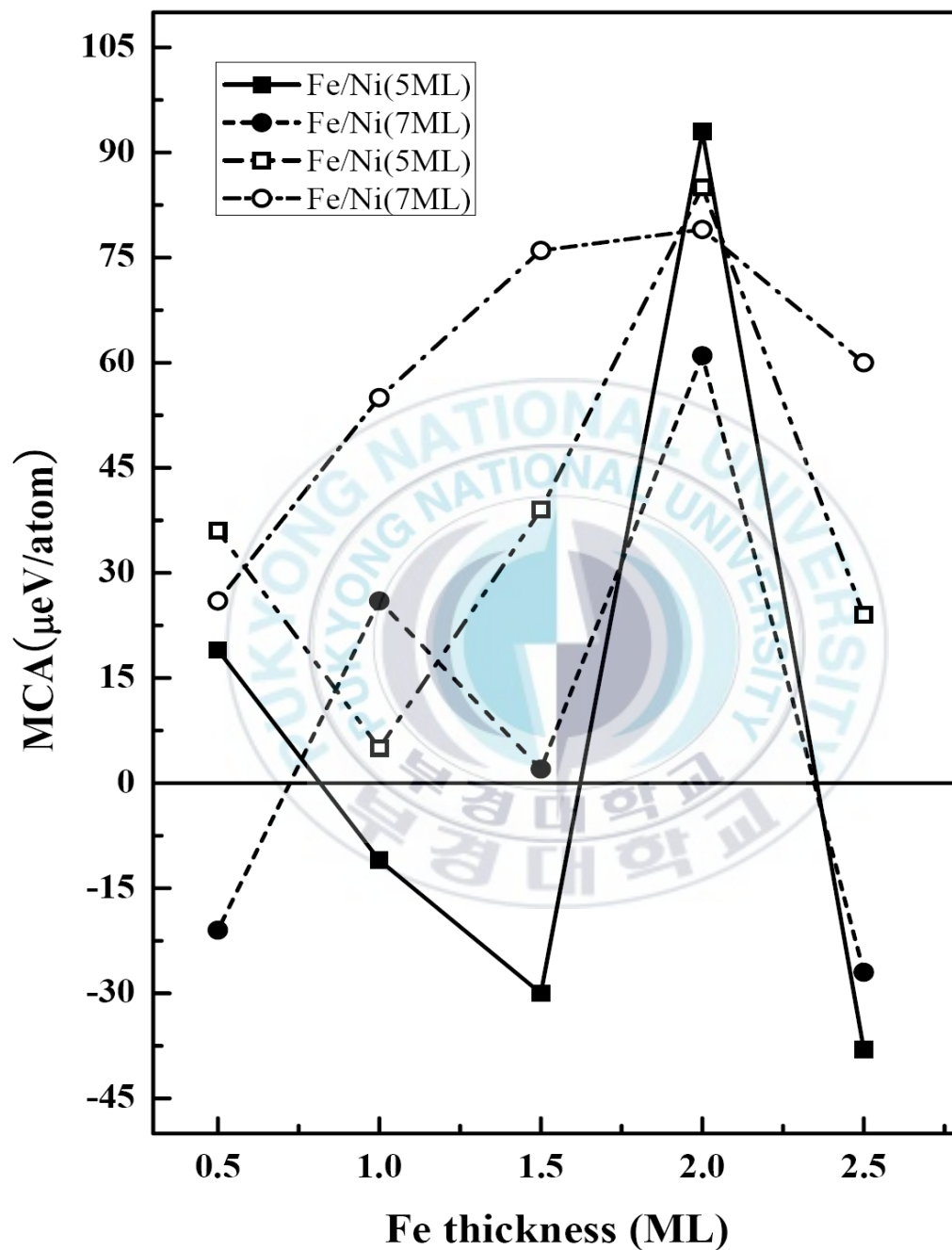


Fig. 4-6. Calculated magnetic anisotropy energy per transition metal atom.

respectively. From these calculations, we can understand the influence both of strain and the Ni thickness dependence for the magnetic anisotropy. In Fig. 4-6, we present the calculated MAE per transition metal atom. The positive MAE means for perpendicular magnetization to the film surface, whereas the negative MAE is for in-plane magnetization. The open symbols are the MAE when the Fe/Ni film is assumed to be grown with Cu(001) lattice constants, whereas the solid symbols are for films with Ni(001) lattice constants. As shown, we have obtained that the Fe/Ni film has always a perpendicular magnetization if the film grows with Cu(001) lattice constant although the magnitude of MAE varies with film thickness. In the presence of strain effect the Fe/Ni(5 ML) films (solid squares) still maintain perpendicular magnetization, but interestingly the spin reorientation transition (SRT) from out-of-plane to in-plane magnetization arises up to 1.5ML Fe coverage. We also see the SRT twice between 1.5 and 2 ML coverage. In contrast, the Fe/Ni(7 ML) has an in-plane magnetization when the Fe coverage is 0.5 ML and the SRT from in-plane to perpendicular magnetization is maintained until 2 ML Fe coverage. As shown in Tables 1 and 2 the magnetic moments of Fe and Ni atoms are insensitive to the strain effect, but it has been found that the magnetic anisotropy is significantly altered due to the strain. Indeed, we have realized that the interpretation of magnetic anisotropy in terms of simple physical quantity such as orbital anisotropy is not suitable. Conventionally, the competitions among bulk, surface, and interface contributions to the magnetic anisotropy in two dimensional film system are discussed. However, the validity of this approach is questionable for ultrathin film since there is no clear separation among those regions. One may also argue that the shape anisotropy contribute to the magnetic anisotropy.

Traditionally, the continuum model for thin film structure has been employed. In Table 4-4, we provide the calculated shape anisotropy and total

magnetocrystalline anisotropy energies for comparison. Here, the Fe/Ni films are assumed to grow with Cu(001) lattice parameters. One can see that the shape anisotropy energy is comparable, for instance in 2.5 ML Fe coverage the shape anisotropy energy is larger than magnetocrystalline anisotropy energy. We should remark that the calculations for shape anisotropy is based on continuum model. Thus, it is assumed that the magnetization is uniformly distributed over the entire volume and the ultrathin films are very flat. However, the magnetization is not uniform as shown in Tables 4-2 and 4-3. Furthermore, the continuum model itself may not be applicable for ultrathin films [3]. Thus, the results should be considered as just rough estimation of shape anisotropy energy.

Hence, one needs to consider the contribution to the magnetic anisotropy at each k-point in two dimensional Brillouin zone (BZ). We have checked the distribution of MAE along the high symmetry directions and found that it is not sufficient to understand the magnetic anisotropy with those sampled points. In Figs. 4-7, we thus present the distribution of magnetic anisotropy in entire two dimensional Brillouin zone. The red circles denote the contributions to the perpendicular magnetization at the specific k-point, while the blue ones are for the contributions to the in-plane magnetization. The size of circle is proportional to the magnitude of magnetic anisotropy energy. In Figs. 4-7(a) and (b), the distributions of MAE for the Fe/Ni(5 ML) and Fe/Ni(7 ML) with Cu(001) lattice constant are presented, while Figs. 4-7(c) and (d) are for Fe/Ni(5 ML) and Fe/Ni(7 ML) with Ni(001) lattice parameter, respectively. In Fig. 4-7(a), one can clearly see that large portion of BZ contributes to the perpendicular magnetization, whereas the major contributions to the in-plane magnetization appears near the zone center ( $\Gamma$  point). With increasing Ni underlayer from 5 to 7 ML the spin-orbit interaction has very different character as displayed. The most significant changes occur approximately within the area of radius  $2\pi/a$  and

around the corner of BZ. Summing up these two counteracting effects, it turns out that the final direction of magnetization is perpendicular to the film surface. In the presence of strain effect the Fe/Ni(5 ML) still has a perpendicular magnetization as shown in Fig. 4-7(c). Compared with Fig. 4-7(a) for Fe/Ni(5 ML) with Cu(001) lattice parameter, we have found that the major changes arise near the BZ center although both systems has the same magnetization direction. Comparing both Figs. 4-7(b) and (d) one can easily note that the strong in-plane contribution around the corner of BZ vanishes, but the strong perpendicular contributions (red circles) disappear as well in the presence of strain. Especially, the area of radius  $2\pi/a$  used to have perpendicular contribution maintains in-plane contribution. These results show that the magnetic anisotropy of ultrathin film with the low coverage as investigated here is significantly modified according to its environment such as interface geometry and these feature many account for the disparity occurred in two experimental data [10,11].

Fe Coverage	0.5 ML	1 ML	1.5 ML	2 ML	2.5 ML
$E_{sh}$	222	181	456	173	757
$E_{MCA}$	246	229	756	436	723

**Table 4-4.** Calculated total shape anisotropy energies ( $E_{sh}$ ) and magnetocrystalline anisotropy energies ( $E_{MCA}$ ) in  $\mu\text{eV}$  for 7 layers of Ni surface systems.

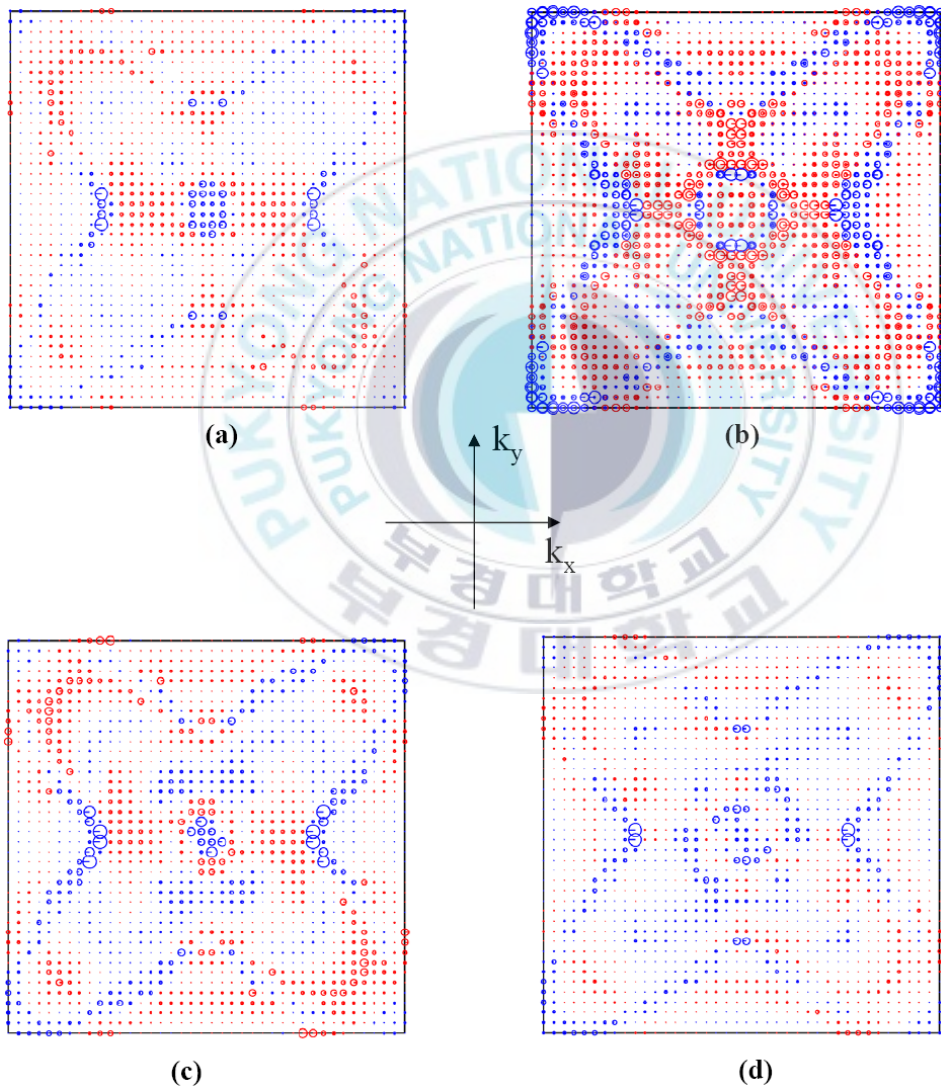


**Fig. 4-7.** Distribution of magnetic anisotropy over two dimensional BZ for 0.5 ML Fe coverage with (a) Fe/Ni(5 ML) with Cu(001) lattice, (b) Fe/Ni(7 ML) with Cu(001) lattice, (c) Fe/Ni(5 ML) with Ni(001) lattice, (d) Fe/Ni(7 ML) with Ni(001) lattice.

## 4.2.5 XMCD and Sum Rule

To explore magnetic properties of materials, the XAS and XMCD tools have been widely employed because one can extract magnetic information of specific element. In our calculations, the dipole transition is only considered and the core-hole relaxation is assumed to be rigid. Therefore, the exact peak position should be shifted if one wants to compare with experimental data. In Figs. 4-8(a) and (b), we show the calculated XAS and XMCD of Fe and surface Ni atoms in 1 ML Fe coverage with 5 ML Fe underlayer, respectively. The dotted lines are for pseudomorphic growth and the solid lines denote the XAS and XMCD spectra in the presence of strain effect. One can see that the strain has no meaningful influence on the XAS and XMCD signals. Both  $L_3$  and  $L_2$  edges of  $Fe_1$  and  $Ni_s$  atoms are well separated and this is a common feature observed in most of studies. In Fig. 4-9 (a), (b) and (c), we display the results, XMCD and XAS spectra, of  $Fe_2$ ,  $Fe_1$  and  $Ni_s$  in 2 ML of Fe coverage, respectively. With increasing Fe coverage the main peak structure of  $Ni_s$  atom is almost unchanged, but the Fe atom show thickness dependent behaviors. For instance, both  $L_3$  and  $L_2$  edges of  $Fe_1$  in 1 ML Fe coverage have well pronounced single peak structure. whereas we have observed double peak feature in 2 ML Fe coverage. Moreover, the top Fe layer ( $Fe_2$ ) also has different behavior from  $Fe_1$ . Indeed, the DOS characters can nicely account for the calculated XAS and XMCD spectral shapes.

The interpretation of XMCD spectra is based on following orbital and spin sum rules.

$$\frac{I_m = \int_{L_3+L_2} \sigma_m dE}{I_t = \int_{L_3+L_2} \sigma_t dE} = \frac{\langle L_z \rangle / 2}{N_h} \quad (4-1)$$

$$\frac{I_s = \int_{L_3+L_2} \sigma_{m, L_3} - 2\sigma_{m, L_2} dE}{I_t = \int_{L_3+L_2} \sigma_t dE} = \frac{(\langle S_z \rangle + 7\langle T_z \rangle) / 3}{N_h} \quad (4-2)$$

Where  $\sigma_m = \sigma_+ - \sigma_-$ ,  $\sigma_t = \sigma_+ - \sigma_- + \sigma_z$ , and the  $T_z$  is the spin magnetic dipole moment. The  $N_h$  can be obtained by integrating over the unoccupied valence states. Nonetheless, the extensive studies for the general validity XMCD sum rule are rather rare although many experimental data interpreted based on that sum rule. Thus, it will be of interest to investigate the usefulness of sum rule based on *ab initio* method. We now present sum rule errors of Fe/Ni films grown on 5 ML of Ni underlayer in the presence of strain effect. The left hand sides in Eqs, (4.1) and (4.2) are obtained from XAS and XMCD spectral shapes and the right hand sides are achieved from *ab initio* calculations. In Table 4- , we present sum rule errors of Fe/Ni films grown on 5 ML of Ni underlayer. The numbers in parenthesis stand for the errors in the presence of strain effect. Here, we check the sum rule errors arising from orbital part, spin part, and the total error separately obtained from the orbital sum rule error

$$R_o = \frac{I_m/I_t}{\langle L_z \rangle / 2N_h} - 1, \text{ the spin sum rule error } R_s = \frac{I_s/I_t}{(\langle S_z \rangle + 7\langle T_z \rangle) / 3N_h} - 1,$$

$$\text{and the total sum rule error } R_t = \frac{I_m/I_s}{\langle L_z \rangle / 2\langle S_e \rangle} - 1 \text{ where}$$

$\langle S_e \rangle = (\langle S_z \rangle + 7 \langle T_z \rangle) / 3$ . First of all, it has been observed that the strain no meaningful influence on the sum rule accuracy and this could be understood from the calculated XAS and XMCD spectra. One can also see that the sum rule is quite reliable in most cases. Nonetheless, the sizable sum rule error in  $R_t$  is found in certain structure, for instance the  $Ni_s$  atoms in 1 ML, 1.5 ML, and 2 ML Fe coverage have about 20% error, but the  $Ni_s$  atoms in 0.5 ML and 2.5 ML have less than 10% error. In contrast, the sum rule error of Fe atom is quite small for all systems. Very interestingly, the separately calculated sum rule error arising from spin ( $R_s$ ) or orbital ( $R_o$ ) part is always sizable in most of systems, but the total error, which is combination of these two components, is significantly suppressed. This feature stems from the denominator in Eqs. (4.1) and (4.2), *i.e.* the  $I_t$  related to the number of holes plays an crucial role in the accuracy of sum rule. As shown in Eqs. (4.1) and (4.2), the error of  $N_h$  enters into the  $I_o$  and  $I_s$  if one considers the error separately and this causes the sizable sum rule error. However, the cancelation of  $I_t$  occurs in total error  $R_t$  and this results in suppression of sum rule error although the sizable inaccuracy from each component is observed. Indeed, it has been suggested that the XMCD sum rule can be improved using the combined form, not employing spin and orbital sum rules separately [19].

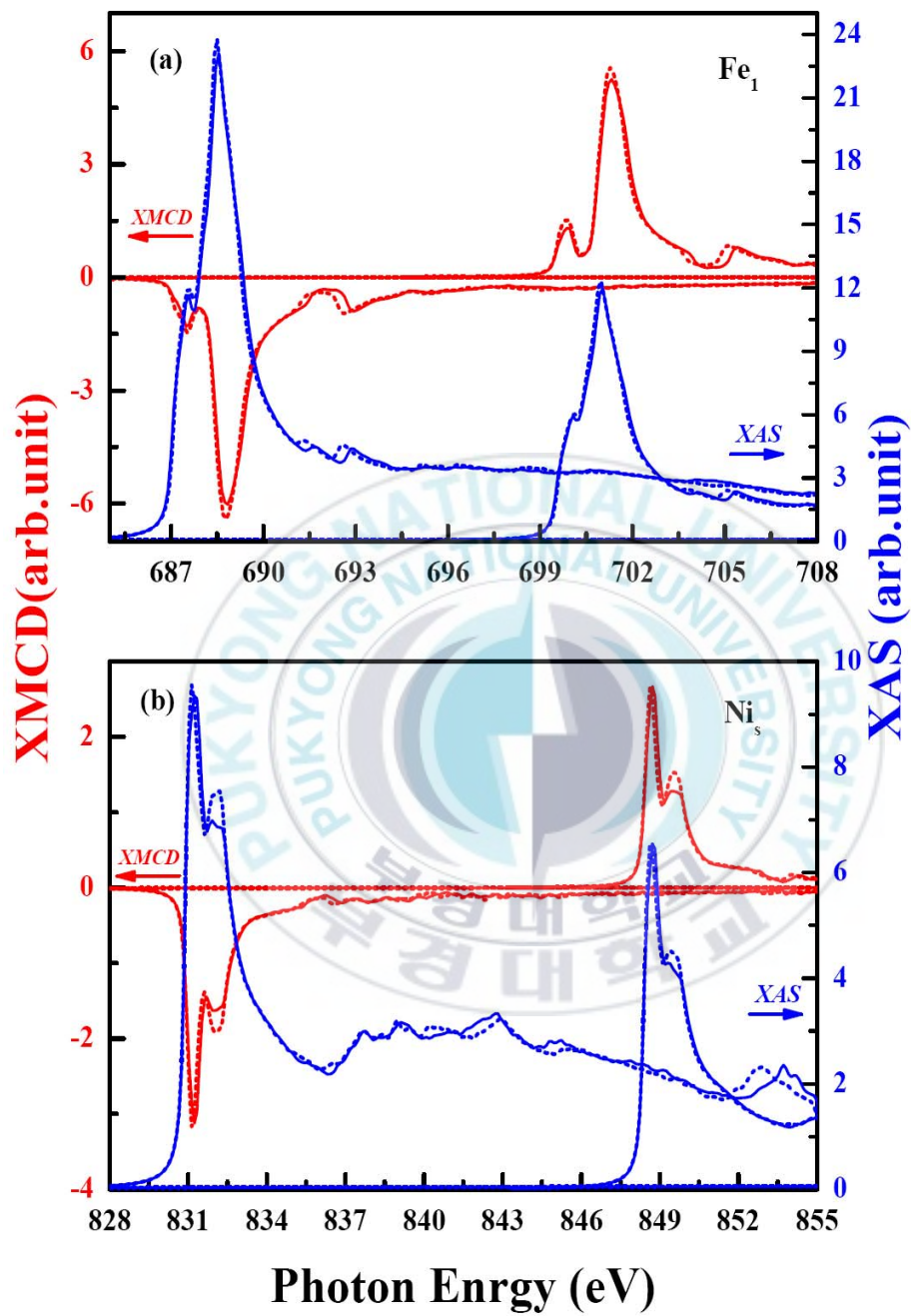


Fig. 4-8. XMCD and XAS spectra of (a)Fe<sub>1</sub> and (b)Ni<sub>5</sub> for Ni 5ML.

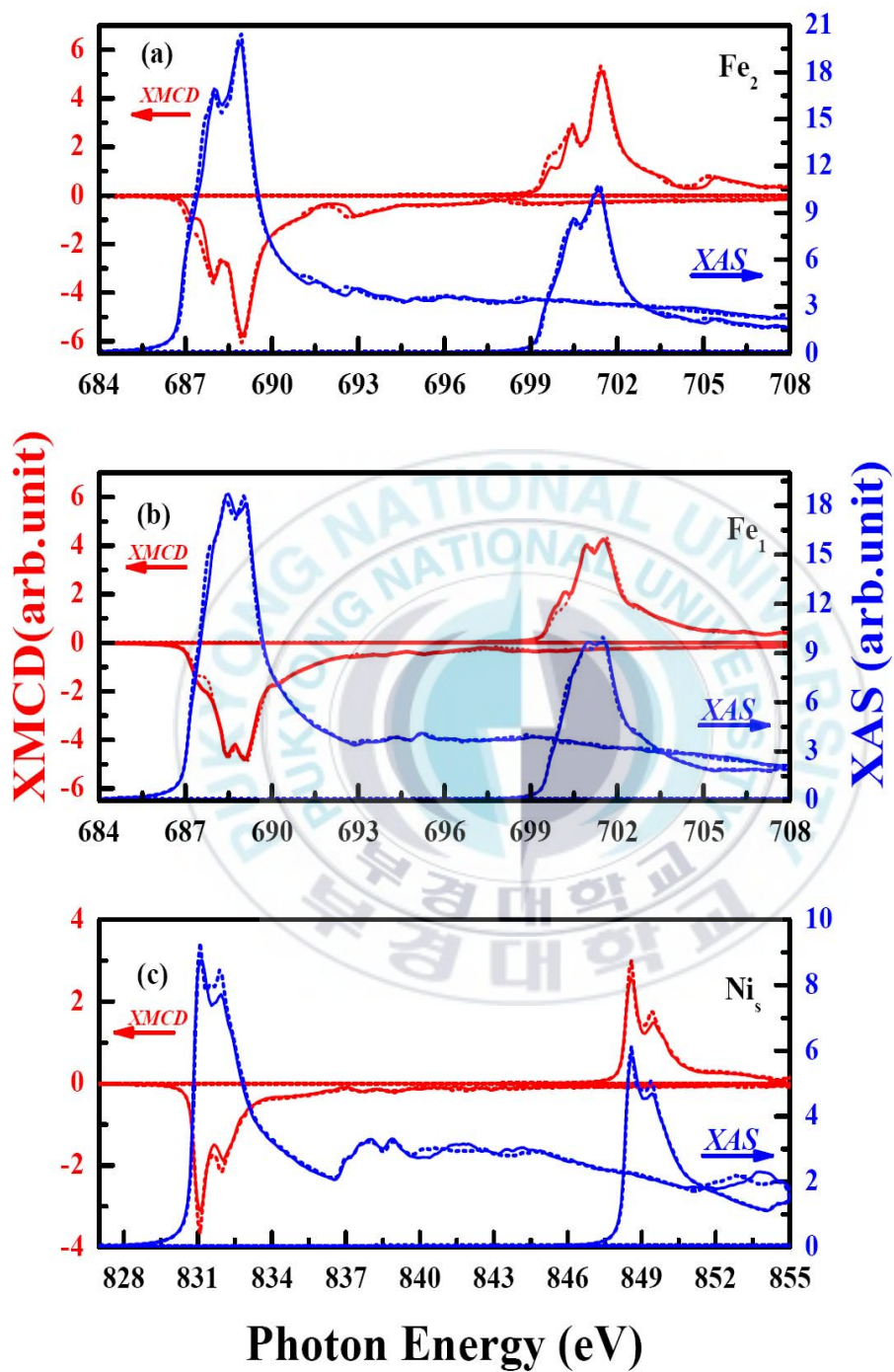


Fig. 4-9. XMCD and XAS spectra of (a)Fe<sub>2</sub>, (b)Fe<sub>1</sub>, and (c)Ni<sub>s</sub> for Ni 5ML.

Fe thickness	atom	$R_o$	$R_s$	$R_t$
0.5 ML	Fe <sub>1</sub>	-0.05 (-0.04)	-0.06 (-0.06)	0.01 (0.01)
	Ni <sub>s</sub>	-0.16 (-0.18)	-0.08 (0.08)	-0.08 (-0.10)
1 ML	Fe <sub>1</sub>	-0.08 (-0.16)	-0.11 (-0.19)	0.04 (0.04)
	N <sub>i</sub>	-0.29 (-0.31)	-0.08 (-0.10)	-0.22 (-0.23)
1.5 ML	Fe <sub>2</sub>	-0.06 (-0.05)	-0.01 (-0.06)	-0.04 (0.02)
	Fe <sub>1</sub>	-0.19 (-0.18)	-0.12 (-0.13)	-0.07 (-0.05)
	Ni <sub>s-a</sub>	-0.17 (-0.18)	-0.14 (-0.14)	-0.04 (0.02)
	Ni <sub>s-b</sub>	-0.19 (-0.12)	-0.15 (-0.25)	-0.05 (0.17)
2 ML	Fe <sub>2</sub>	-0.04 (-0.06)	-0.11 (-0.13)	0.08 (0.08)
	Fe <sub>1</sub>	-0.06 (-0.06)	-0.14 (-0.14)	0.08 (0.08)
	Ni <sub>s</sub>	-0.31 (-0.31)	-0.14 (-0.13)	-0.20 (-0.21)
2.5 ML	Fe <sub>3</sub>	-0.05 (-0.03)	-0.08 (-0.06)	0.03 (0.04)
	Fe <sub>2</sub>	-0.19 (-0.19)	-0.12 (-0.12)	-0.07 (-0.07)
	Fe <sub>1-a</sub>	-0.22 (-0.21)	-0.15 (-0.15)	-0.08 (-0.07)
	Fe <sub>1-b</sub>	-0.19 (-0.20)	-0.14 (-0.14)	-0.05 (-0.06)
	Ni <sub>s</sub>	-0.19 (-0.20)	-0.15 (-0.15)	-0.05 (-0.07)

**Table 4-5.** Calculated sum rules error. The numbers in parenthesis stand for the errors in the presence of strain effect.

### 4.3 Conclusion

In conclusion, we have investigated the magnetic properties of Fe/Ni/Cu(001) films varying both thickness of Fe adlayer and Ni underlayer including the strain effect. It has been found that the spin magnetic moments are less sensitive to the strain effect. For the top Fe adlayer a sensitive to the strain effect. For the top Fe adlayer a typical surface enhancement of spin magnetic moment is found and the half metallic state is observed. From the magnetic anisotropy calculations, we have found that the Fe/Ni have perpendicular magnetization to the surface. However, the direction of magnetization changes in the presence of strain and it is also dependent on the Fe film thickness. These results imply that the magnetic anisotropy may strongly depend on the interface structure or growing mode in the presence of very low adatom coverage, thus it is of necessity to identify the structure of film for understanding the SRT phenomenon.

Nonetheless, the XAS and XMCD spectral shape show almost the same trend even in the presence of strain effect. Through the sum rule calculations, we have found that the sum rule error of Fe atom is quite satisfactory, but the Ni<sub>s</sub> atom shows rather large error in some cases. Interestingly, we suggest that the sum rule can be improved by combining the spin and orbital sum rules, whereas the sum rule form each component has sizable error.

## Reference

- [1] B. Schulz and K. Baberschke, Phys. Rev. B 50, 13467 (1994).
- [2] W.L. O'Brien and B.P. Tonner, Phys. Rev. B 49, 15370 (1994).
- [3] K. Baberschke, in *Band ferromagnetism*, edited by K. Baberschke, M. Donath, and N. Nolting (Springer Berlin, Berlin 2001), and reference therein.
- [4] S. Hope, E. Gu, B. Choi, and J.A.C. Bland, Phys. Rev. Lett. 80, 1750 (1998)
- [5] R. Vollmer, Th. Gutjahr-Löser, J. Kirschner, S. van Dijken, and B. Poelsema, Phys. Rev. B 60, 6277 (1999).
- [6] S. van Dijken, R. Vollmer, B. Poelsema and J. Kirschner, J. Magn. Mater. 210, 316 (2000).
- [7] Jisang Hong, R.Q. Wu, J. Lindner, E. Kosubek, and K. Baberschke, Phys. Rev. Lett. 92, 147202 (2004)
- [8] X. Liu and M. Wutting, Phys. Rev. B 64, 104408 (2001).
- [9] R. Ramchal, A.K. Schmid, M. Farle, and H. Poppa, Y. Mo, K. Varga, E. Kaxiras, and Z. Zhang, Phys. Rev. B 69, 214401 (2004).
- [10] R. Thamankar, S. Bhagwat, F.O. Schumann, J. Magn. Mater. 281 (2004) 206.
- [11] H. Abe, K. Amemiya, D. Matsumura, S. Kitagawa, H. Watanabe, T. Yokoyama, T. Ohta, J. Magn. Mater. 86 (2006) 302.
- [12] Dongyoo Kim and Jisang Hong, J. Magn. Mater., (in press).
- [13] S. Chikazumi. Physics of Ferromagnetism. Oxford Science Publications, New York 1978.
- [14] R. Pauthenet, Y. Barnier, and G. Rimet, J. Phys. Soc. Japan, 17 Suppl. B-I (1969), 309.
- [15] H. Gengnagel and U. Hofmann, Phys. Stat. Sol., 29 (1968), 91.

- [16] J. J. M. Franse and G. de Vries, *Physica*, 39 (1968), 477.
- [17] J. Stöhr, *J. Mag. Mag. Mat*, 200, 470 (1999)
- [18] J. Stöhr, Y. Wu, in: A.S. Schlachter, F.J. Wuilleumier (Eds.), *New Directions in Research with Third-Generation Soft X-Ray Synchrotron Radiation Sources*, Kluwer Academic Publishers, Netherlands, 1994, p. 221.
- [19] J. Stöhr, *J. Electron. Spectrosc. Relat. Phenom.* 75 253 (1995).
- [20] J. Stöhr, R. Nakajima, *IBM J. Res. Develop.* 42 73 1998).
- [21] E. Wimmer, H. Krakauer, M. Weinert, A.J. Freeman, *Phys. Rev. B* 24 (1981) 864.
- [22] E. Wimmer, H. Krakauer, M. Weinert, A.J. Freeman, *Phys. Rev. B* 26 (1981) 4571.
- [23] M. Weinert, *J. Math. Phys.* 22 (1981) 2433.
- [24] J. C. Slater, *Phys. Rev.* 51 (1937) 846.
- [25] D. D. Koelling and G. O. Arbman, *J. Phys. F* 5, (1975) 2041.
- [26] O. K. Andersen, *Phys. Rev.* 12 (1975) 3060.
- [27] H. J. F. Jansen and A. J. Freeman, *Phys. Rev.* 30 (1984) 561.
- [28] E. Wimmer, H. Krakauer, M. Weinert, and A. J. Freeman, *Phys. Rev. B* 24(1981) 864; references therein.
- [29] P. Hohenberg and W. Kohn, *Phys. Rev.* 136 (1964) B864.
- [30] W. Kohn and L. J. Sham, *Phys. Rev.* 140 (1965) A1133.
- [31] M. Born and R. Oppenheimer, *Ann. Phys. Lpz.* 84 (1927) 124.
- [32] J. P. Perdew, J. A. Chevary, S. H. Vosko, K. A. Jackson, M. R. Pederson, D. J. Singh, and C. Fiolhais, *Phys. Rev. B* 46, 6671 (1992).
- [33] B. G. Johnson, P. M. W. Gill, and J. A. Pople, *J. Chem. Phys.* 98, 5612 (1993).

[44] A. D. Becke, in the challenge of d and f Electrons, ACS symposium series No. 394, eds.

D. R. Salahub and M. C. Zerne (American chemical society, Washington, DC, 1989), p. 165.

[35] A. Garcia, C. Elsaesser, J. Zhu, S. Louie, and M. L. Cohen, Phys. Rev. B 46, 9829 (1992).

[36] Y. M. Juan, E. Kaxiras, and R. G. Gordon, Phys. Rev. B 51, 9521 (1995)

[37] A. Dal Corso, A. Pasquello, A. Baldereshi, and R. Car, Phys. Rev. B 53, 1180 (1996).

[38] M. Körling and J. Häglund, Phys, Rev. B 45, 13293 (1992).

[39] B.T. Thole, P. Carr, F. Sette, and G. van der Laan, Phys. Rev. Lett. 61, 1943 (1992).

[40] P. Carr, B.T. Thole, M. Altarelli, and X.D. Wang, Phys. Rev. Lett. 70, 694 (1993)

[41] J. P. Perdew, K. Burke, M. Ernzerhof, Phys. Rev. Lett. 77 (1996) 3865.

[42] X.D. Wang, R.Q. Wu, D.S. Wang, A.J. Freeman, Phys. Rev. B 54 (1996) 61.

[43] R. Vollmer, Th. Gutjahr-Löser, J. Kirschner, S. van Dijken, and B. Poelsema, Phys. Rev. B 60, 6277 (1999).

# 답례의 글

2년이라는 시간, 그리고 여러분의 도움과 가르침을 거름으로 삼아, 이렇게 석사 과정을 마무리 하게 되었습니다. 여러분의 도움과 가르침에 글로써 짧게 남아 감사를 드리고자 합니다.

먼저, 저의 지도 교수님이신 홍지상 교수님에게 감사를 드립니다. 2년 동안 물리에 대한 지식과 연구 방법에 대한 많은 가르침은 이 논문을 완성함에 있어 가장 필수적인 그것이었습니다. 이러한 교수님의 가르침이 제 앞날의 중요한 밑거름이 될 것임을 믿어 의심치 않습니다.

바쁘신 와중에도 멀리 대전에서 부산까지 오셔서 논문 지도를 해주신 황찬용 박사님께 마음 깊은 고마움을 전하고 싶습니다. 아울러 학부 과정과 석사 과정 동안 좋은 강의와 함께 저의 궁금증을 풀어 주시고, 논문 지도 해 주신 문병기 교수님께도 고마움을 전합니다.

항상 저의 나태해지는 마음가짐에 긴장을 불러 넣어주셨던 이종규 교수님에게 감사의 말씀 전합니다. 그리고 항성 저희에게 좀 더 좋은 강의를 해주시려 열성을 다해주신 김성부 교수님께 깊은 감사함을 전합니다. 교수님의 열정을 보고, 느끼며 공부해온 시간은 참으로 좋은 시간이었습니다.

이제, 선배님들과 친구들 그리고 후배님들에게 고마움을 표하려 합니다. 먼저, 항상 저에게 조언을 아끼지 않으셨던 승일 선배, 규성 선배, 경혁 선배, 그리고 일민 선배에게 감사의 말을 전합니다. 학부 때부터 항상 토론하며 서로를 격려하고 충고해준 우리 99학번 동기들, 대길, 태선, 세원, 은식, 경희에게 고마움을 보냅니다. 그리고 대학원 생활에 많은 도움을 준 순길, 현경에게도 고마움을 전합니다. 또한, 재민, 진영, 종원, 홍채, 그리고 같은 연구실에서 동거 동락하는 용특 에게도 짧은 글로 고마움을 대신합니다.

마지막으로, 아들이 하는 일이라면 항상 믿어주시는 아버지와 어머니, 항상 동생 과 처남 걱정해주시는 누나와 매형, 우리 막내 동생 이경이 에게도 사랑한다는 말과 함께 깊은 고마움을 전합니다.

2008년 1월

김동유 올림